The Radio Occultation (ROC) Instrument

1. Balloon GPS RO measurements technique

GPS Radio Occultation (RO) senses the atmosphere using radio signals that traverse the atmosphere as a transmitting GPS satellite sets behind the horizon relative to a moving receiver. The radio wave undergoes refractive bending and a Doppler shift due to variations of the atmospheric refractive index. We have developed GPS Radio Occultation (RO) instrumentation for both aircraft (Garrison et al. 2007; Haase et al. 2014; Murphy et al. 2015; Xie et al. 2008) and for superpressure balloons for the Concordiasi campaign in Antarctica (Haase et al. 2012).

The refractive index of the neutral atmosphere depends on pressure, temperature, and humidity, and is given by (Smith and Weintraub 1953)

Figure 1 Schematic diagram of airborne RO geometry. Red dots are tangent point locations (point closest to surface).

$$N = (n-1) \times 10^6 = 77.6\frac{P}{T} + 3.73 \times 10^5 \frac{P_w}{T^2} \qquad (1)$$

where N is refractivity, n is the refractive index, P is pressure [hPa], T is temperature [K], and P_w is water vapor partial pressure [hPa]. Geometric optics retrieval techniques assume spherical symmetry to map the atmospheric delay along the raypath to refractivity at the tangent point location, the point of closest approach to the Earth surface (Figure 1). Retrieval of moisture and temperature from RO observations, assuming spherical symmetry of the atmosphere, for the case of spaceborne sounding is fully described in (Kursinski et al. 1997; Melbourne et al. 1994; Vorobe'ev and Krasil'nikova 1994), with modifications and implementation for the airborne and balloon-borne cases described in (Haase et al. 2012; Haase et al. 2014; Healy et al. 2002; Xie et al. 2008).

2. Sampling characteristics of ROC

Because the GPS satellite velocity is much greater than the balloon velocity, the tangent point drifts horizontally away from the balloon as the GPS satellite sets. The sampling characteristics of ROC are listed in Table 1. Figure 2 shows the expected geometric distribution of occultations, using a simulation based on a Pre-Concordiasi equatorial flight, that also illustrates the horizontal extent of each individual occultation profile as the tangent point descends lower in the atmosphere and samples points further from the balloon path. Figure 3 and Figure 4 illustrate the expected sampling of a wave generated temperature perturbation in the atmosphere by the ROC sample point distribution over the course of one day.

Table 1 Sampling characteristics for the balloon-borne ROC system.

Vertical resolution	200-250 m
Horizontal resolution	70% of the signal is accumulated within +/- 50 km of the tangent point at 10km height
Duration of occultations	17 minutes
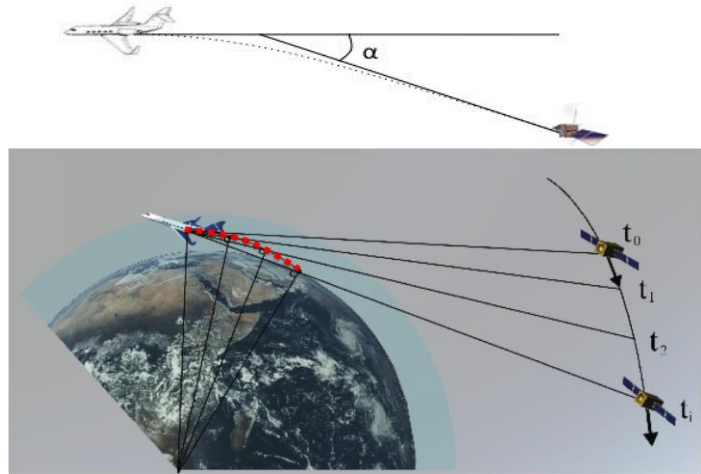
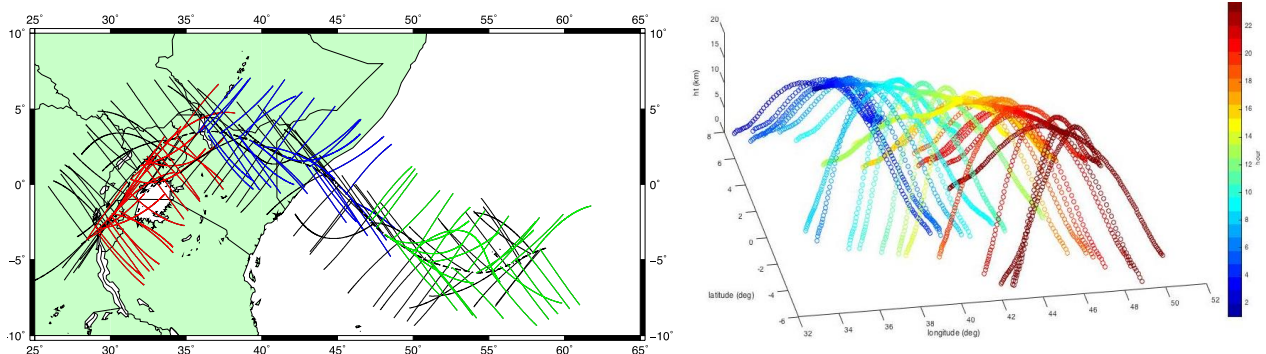| Frequency of occultations	~2.5 per hour
Expected number of occultations per day	~30 setting and ~6-10 rising per day per balloon
Upper limit of useful measurements	~flight altitude (~20 km)
Lower limit of useful measurements	~7-8 km in the tropics
Accuracy	<2% refractivity
Max. horizontal distance	450 km from tangent point from flight path

Figure 2 (left) Prediction of occultations that would be obtained over three days (13 Mar setting, 14 Mar setting, and 15 Mar setting) assuming a Pre-Concordiasi flight trajectory. Rising occultations are in black. (right) perspective view of the tangent point locations for profiles on day 073, color shows observation time.
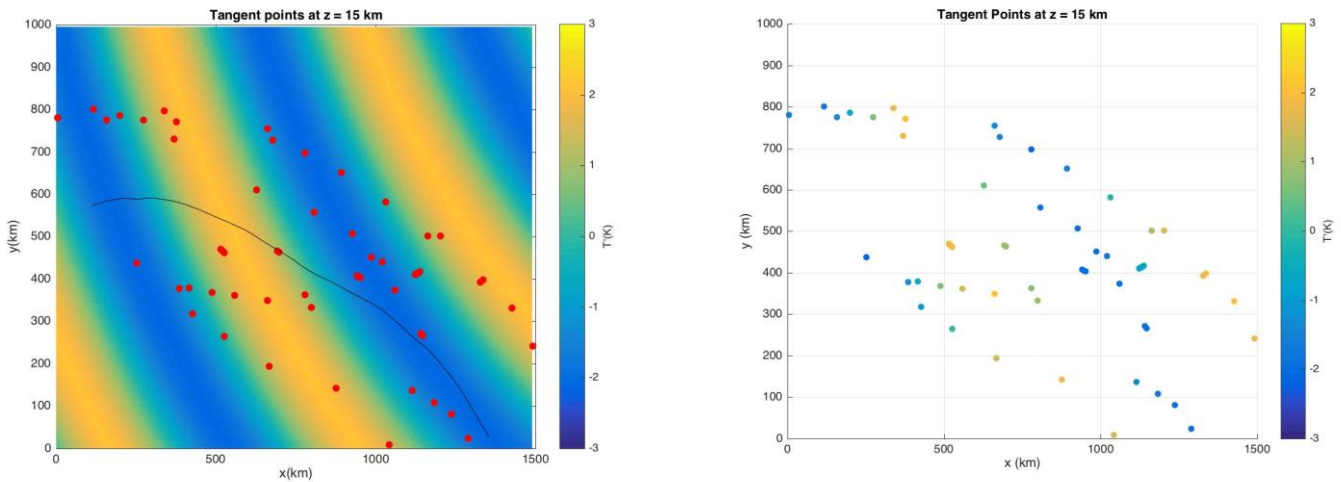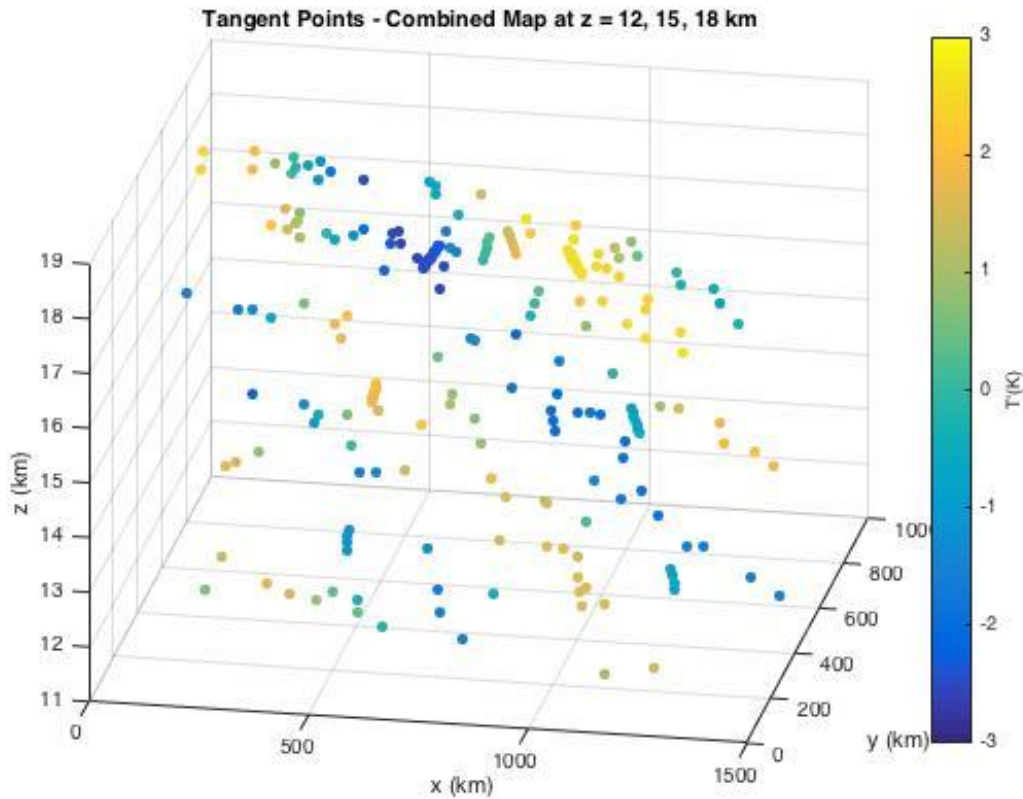

Figure 3 Horizontal temperature perturbation from an idealized 600 km wavelength wave with tilted phase structure at 18 km (top), 15 km (center) and 12 km (lower panels). Black line is the simulated balloon trajectory, red points are locations of the occultation tangent points from all of the profiles that occur over the course of a day at the corresponding height. At right are the same occultation points where the color of the symbol corresponds to the temperature anomaly at that point.

Figure 4 Perspective view of the sampling of temperature perturbation T' in 3D.

3. ROC instrument

The Radio Occultation instrument system (ROC) will be based on the successful design used in the Concordiasi campaign in Antarctica (Figure 5; Figure 6). The package is comprised of one Septentrio AsteRx4 multiGNSS receiver OEM board connected to a dedicated Aero AT2775-41F avionics antenna with a 40dB preamplifier. The GNSS receiver board is managed by a single board computer (ie the Technologic Systems *TS-7260*) with onboard software to control startup, shutdown, configuration, command and control, local data recording, compression, and communication. The instrument will interface with the new Zephyr gondola designed by the Laboratoire de Metéorologie Dynamique (LMD) and an Iridium RUDICS communication modem for data transmission to the Mission Control Center at LMD. The capabilities of the OEM board in extremely cold environments have been evaluated by UNAVCO, the NSF facility for GPS geodesy infrastructure. The new receiver has advanced capabilities compared to the previous version of ROC, including tracking GLONASS and GALILEO occultations, which essentially could triple the number of occultations available. Following analysis of the final power and data budgets, this additional capability will be implemented for intense observation periods.
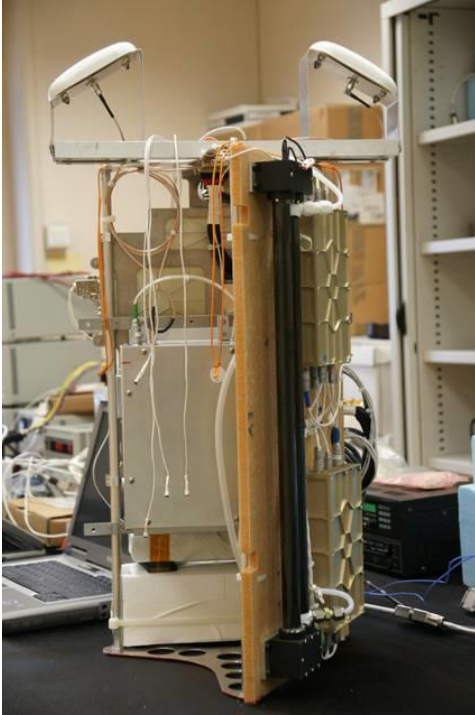
Figure 5 ROC flight model PSC18 from Concordiasi with two antennas and two receivers.
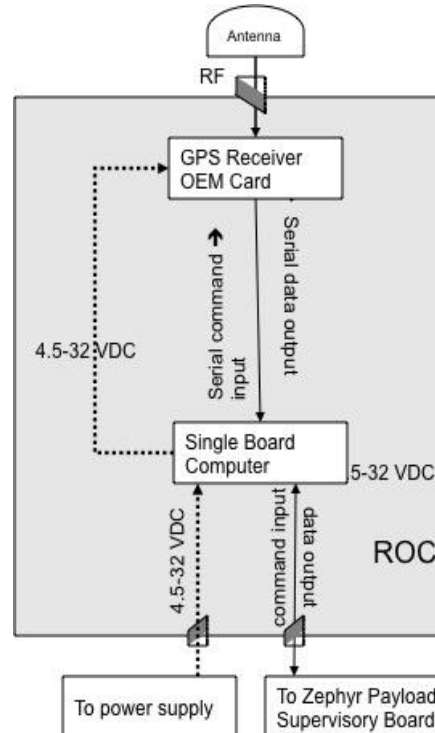
Figure 6 Block diagram of ROC system for Strateole-2 with a single antenna and receiver board.

4. References

Garrison, J.L., Walker, M., Haase, J.S., Lulich, T., Xie, F., Ventre, B.D., Boehme, M.H., Wilmhoff, B. & Katzberg, S.J. 2007. Development and Testing of the GISMOS Instrument. Proceedings of the IEEE International Geoscience and Remote Sensing Symposium, 1-4.

Haase, J.S., Maldonado-Vargas, J., Rabier, F., Cocquerez, P., Minois, M., Guidard, V., Wyss, P. & Johnson, A.V. 2012. A proof-of-concept balloon-borne Global Positioning System radio occultation profiling instrument for polar studies. Geophysical Research Letters, **39**, doi: L02803 10.1029/2011gl049982.

Haase, J.S., Murphy, B.J., Muradyan, P., Nievinski, F., Larson, K.M., Garrison, J.L. & Wang, K.-N. 2014. First Results from an Airborne GPS Radio Occultation System for Atmospheric Profiling. Geophysical Research Letters, **40**, doi: 10.1002/2013GL058681.

Healy, S.B., Haase, J. & Lesne, O. 2002. Abel transform inversion of radio occultation measurements made with a receiver inside the Earth's atmosphere. Annales Geophysicae, **20**, 1253-1256.

Kursinski, E.R., Hajj, G.A., Hardy, K.R., Schofield, J.T. & Linfield, R. 1997. Observing Earth's atmosphere with radio occultation measurements. J. Geoph. Res., **102**, 23.429-423.465.

Melbourne, W.G., Davis, E.S., Duncan, C.B., Hajj, G.A., Hardy, K.R., Kursinski, E.R., Meehan, T.K., Young, L.E. & Yunck, T.P. 1994. *The application of spaceborne GPS to atmospheric limb sounding and global change monitoring.* Jet Propulsion Laboratory Report **94-18**.

Murphy, B.J., Haase, J.S., Muradyan, P., Garrison, J.L. & Wang, K.-N. 2015. Airborne GPS radio occultation refractivity profiles observed in tropical storm environments. Journal of Geophysical Research, **120**, 1690-1790, doi: 10.1002/2014JD022931.

Smith, E.K. & Weintraub, S. 1953. The constants in the equation for atmospheric refractive index at radio frequencies. Proc. IRE,, **41**, 1035-1037.

Vorobe'ev, V.V. & Krasil'nikova, T.G. 1994. Estimation of the accuracy of the atmospheric refractive index recovery from Doppler shift measurements at frequencies used in the NAVSTAR system. Physics of the Atmosphere and Ocean (English Translation), **29**, 602-609.

Xie, F., Haase, J.S. & Syndergaard, S. 2008. Profiling the Atmosphere Using the Airborne GPS Radio Occultation Technique: A Sensitivity Study. Trans. IEEE Geosci. and Remote Sens., **46**, 3424-3435.